Holz als Roh- und Werkstoff (2006) 64: 1–10
DOI 10.1007/s00107-005-0027-2

Heiko Thoemen · Philip E. Humphrey

Modeling the physical processes relevant during hot pressing of wood-based composites. Part I. Heat and mass transfer

Published online: 3 November 2005

Abstract A three-dimensional model based on fundamental principles to simulate heat and mass transfer and mat densification during batch or continuous hot pressing of wood-based composites is presented in this pair of papers. The present paper gives a comprehensive description and mathematical formulation of the relevant heat and mass transfer mechanisms, which are water vapor and air transfer by gas convection and molecular gas diffusion, conductive and convective heat transfer, including sorptive effects. The heat and mass transfer model consists of a set of constitutive flux equations that are coupled by local energy and mass balances.

Material property data used as input parameters for the model are provided for medium density fibreboard (MDF). These properties are highly dependent on one or more of the internal mat conditions, being temperature, moisture content and density. The determination of mat permeability, obstruction factor for molecular diffusion, and thermal conductivity was part of the project described here, while the specific heat, heat of sorption, and hygroscopicity data were taken from the literature. In addition, physical property data for the water vapor-air mixture are listed.

The model may be used as a tool to optimize the manufacture of existing natural fiber composites, to aid in the development of new products and technology for their production, and for training purposes.

Modellierung der physikalischen Vorgänge beim Heißpressen von Holzwerkstoffen. Teil I. Wärme- und Stofftransport

Zusammenfassung In den beiden vorliegenden Artikeln wird ein drei-dimensionales Modell zur Simulation der Wärme- und Stofftransportvorgänge sowie der Materialverdichtung beim Verpressen von Holzwerkstoffen in Takt- oder Doppelbandpressen beschrieben. Der erste Artikel beinhaltet dabei die umfassende Beschreibung und mathematische Formulierung der relevanten Wärme- und Stofftransportvorgänge, das heißt Konvektion des Wasserdampf-Luft-Gemisches, Gasdiffusion der einzelnen Komponenten, sowie konduktiver und konvektiver Wärmetransport unter Einbeziehung von Sorptionsvorgängen. Das Wärme- und Stofftransportmodell besteht aus einem System von Grundgleichungen, die durch lokale Energie- und Massengleichgewichte gekoppelt sind.

Für eine Mitteldichte Faserplatte (MDF) werden Werte für Materialeigenschaften präsentiert, die als Modelleingangsdaten dienen. Die Eigenschaften sind dabei stark abhängig von einem oder mehreren Zustandsparametern des Faservlieses, wie Temperatur, Feuchte oder Dichte. Die Bestimmung der Mattenpermeabilität, der Diffusionswiderstandszahl und der Wärmeleitfähigkeit waren Teil des hier beschriebenen Projektes, während Daten für die Spezifische Wärme, Sorptionswärme und Ausgleichsfeuchte der Literatur entnommen sind. Außerdem werden Werte für die physikalischen Eigenschaften des Wasserdampf-Luft-Gemisches präsentiert.

Das hier beschriebene Modell lässt sich als Werkzeug zur Prozessoptimierung zur Produkt- und Verfahrensentwicklung sowie für Schulungszwecke einsetzen.

H. Thoemen (✉)
Department of Wood Science, University of Hamburg,
Leuschnerstrasse 91, 21031 Hamburg, Germany
E-mail: thoemen@holz.uni-hamburg.de

P.E. Humphrey
Adhesive Evaluation Systems, Inc., 1235 NW Kainui Drive, Corvallis, Or 97330
College of Forestry, Oregon State University, Corvallis, Or 97331-7402, USA

1 Introduction

Hot pressing of the wood-furnish mat plays a crucial role in the production of wood-based composites. The press is the most costly piece of equipment to acquire and operate; thus, it usually determines the maximum capacity of the production line. Moreover, the in-use properties of final products depend heavily on the conditions under which mats are pressed. A fundamental understanding of the pressing process is therefore essential for optimizing production speed, costs, energy consumption, and emissions, as well as for manipulating board properties and developing new technologies and products.

During the last two decades modeling and computer simulation of the hot pressing process have developed as an important tool to generate such fundamental knowledge. Apparently, the first multi-dimensional heat and mass transfer model was developed by Humphrey (1982). Some additional models have been developed during the subsequent two decades. A comprehensive summary of the first generation of models is given by Steffen (1996). Since then, works on integrated models describing the hot pressing process have been presented by Dai and co-workers (Hubert 1998, Dai and Yu 2004), Carvalho and coworkers (Carvalho and Costa 1998, Carvalho et al. 2003), Zombori (2001), Nigro and Storti (2001) and Garcia (2002). Clearly, these models differ with respect to mechanisms included, material type focused on, and predictive power.

The aim of this pair of papers is to outline a comprehensive model that includes those mechanisms most important during hot pressing, and to demonstrate the quality of model predictions possible today. The model described here uses the heat and mass transfer model of Humphrey (1982) and Humphrey and Bolton (1989) as a starting point. The completely revised heat and mass transfer mechanisms have been complemented by a rheological model to account for the localized densification of the wood-furnish mat and for the development and relaxation of internal stresses.

The description and validation of the new process model is divided into two parts. This paper deals with the basic heat and mass transfer mechanisms, while densification and stress relaxation mechanisms are presented in Thömen et al. (2005).

The reported model can be applied to both batch and continuous pressing processes. For convenience, in the present paper the general model description and the boundary conditions are presented only for the batch process, although the relevant physical mechanisms inside the wood-furnish mat apply similarly to both manufacturing processes. Those features of the modeling approach specific to the continuous press have already been described by Thömen and Humphrey (2003). Further, model predictions of inter-fiber bond strength development, based on adhesion kinetics data derived with the ABES technique (Humphrey 1999) and with the IPATES (Heinemann 2004) are not included here; they will be dealt with in separate publications.

The reported research focused mainly on medium density fiberboard (MDF), although, in principle, most of the mechanisms in the model could be applied to other wood furnish materials. Some of the assumptions made in the present model, however, could become problematic with larger wood constituents. Relevant aspects of the model should be reviewed critically and possibly revised before it is applied to OSB and other such materials.

2 Model description

2.1 Summary of model assumptions

Listed below are the most significant assumptions made in the model. A comprehensive problem statement, as well as derivations and justifications of the assumptions made are given in Thömen (2000).

- The material is macroscopically homogeneous.
- Heat and mass transfer takes place in three spatial dimensions.
- Water exists in bound and vapor states; free water is not present.
- Mass transfer of fluids occurs by convection and diffusion of vapor and air; bound water and surface diffusion is negligible.
- Heat is transferred by convection (i.e. gas flow in combination with phase change) and conduction.
- Local equilibrium between gas phase and cell walls is reached instantaneously.

2.2 Mathematical formulation

2.2.1 Constitutive equations for mass transfer

The gas in the porous mat is regarded as a pure two-component mixture of air and water vapor. A convective (or viscous) flux j^{c} of the gas mixture develops in response to a total pressure gradient. This flux is assumed to be laminar (Denisov et al. 1975, Bolton and Humphrey 1994, von Haas et al. 1998) and can be calculated by applying Darcy's law. In addition to this convective flux, a diffusive flux j^{d} occurs due to partial pressure gradients of each of the components; the steady-state diffusive flux can be described by Fick's first law. As both total and partial pressure gradients are generated within the mat during hot pressing, the convective and diffusive fluxes occur simultaneously. It is widely accepted, however, that convective gas flow is the predominant mass transfer mechanism during hot pressing (e.g. Denisov et al. 1975, Gefahrt 1977). Own sensitivity studies (not presented in this paper) confirm the dominance of convective gas flow. The total flux j_i of component i, which can be vapor or air, is given by the following expression:

$$j_i = j_i^{\mathrm{d}} + j_i^{c} \quad i = \mathrm{v, a}\,. \tag{1}$$

The diffusive and convective fluxes, respectively, can be calculated as:

$$j_i^{\mathrm{c}} = -\frac{k_{\mathrm{p}}}{\eta}\frac{M_i}{RT_{\mathrm{abs}}} p_i \nabla p \quad i = \mathrm{v, a} \tag{2}$$

$$j_i^{d} = -D_{\mathrm{eff}}\frac{M_i}{RT_{\mathrm{abs}}} \nabla p_i \quad i = \mathrm{v, a} \tag{3}$$

where v, a = subscripts to denote vapor or air, $j_i^{\mathrm{d,c}}$ = diffusive or convective flux, respectively, of component i [$\mathrm{kg\,m^{-2}s^{-1}}$], D_{eff} = effective diffusion coefficient [$\mathrm{m^2/s}$], M_i = molecular mass of component i [$\mathrm{kg\,mol^{-1}}$], p_i = partial pressure of component i [Pa], p = total gas pressure [Pa], R = gas constant [$\mathrm{J\,mol^{-1}K^{-1}}$], T_{abs} = absolute temperature [K], k_{p} = permeability coefficient [$\mathrm{m^2}$], η = dynamic viscosity of the gas mixture [Pa s], ∇ = gradient operator [$\mathrm{m^{-1}}$].

The effective diffusion coefficient $D_{\mathrm{eff}} = D_{\mathrm{va}}/k_{\mathrm{d}}$ depends on the binary diffusion coefficient D_{va} of the vapor-air gas pair and on the dimensionless obstruction factor k_{d} (Krischer 1963).

2.2.2 Mass conservation equation

For the multi-dimensional problem, the mass conservation equation for the gas component i (i.e., vapor or air) can be expressed in the following way:

$$\underset{\text{(mass flux)}}{-\frac{RT_{\mathrm{abs}}}{M_i}\nabla\cdot j_i} \underset{\text{(compression)}}{- p_i\frac{\partial\phi}{\partial t}} + \underset{\text{(temperature)}}{\frac{p_i\phi}{T_{\mathrm{abs}}}\frac{\partial T}{\partial t}} + \underset{\text{(generation)}}{\frac{RT_{\mathrm{abs}}}{M_i}r_i} = \underset{\text{(pressure)}}{\phi\frac{\partial p_i}{\partial t}}; \quad i = \mathrm{v,\,a}\,. \tag{4}$$

The term on the right hand side of Eq. 4 describes the change in partial pressure p_i of gas component i in an infinitesimally small control region. The dimensionless variable ϕ denotes the void fraction of the porous material (assuming cell wall material is inaccessible to gas). The change in partial pressure depends on each of the four terms on the left hand side. The first one describes the total mass flux j_i of gas component i by convection and diffusion. R, T_{abs} and M_i denote the gas constant, absolute temperature and molecular mass of component i, respectively. The second term on the left hand side accounts for changes in void fraction due to compression (or spring-back) of the mat. The effect of temperature on the partial pressure is expressed in the third term on the left hand side. The fourth term accounts for the generation of component i. The rate of generation, r_i, is zero in the mass conservation equation for air, as it is assumed that there is no interaction between the air and the cell wall substance or other gas components. In the mass conservation equation for vapor, setting r_i equal to m_{ev} accounts for the transformation of vapor into bound-water, or vice versa. The evaporation rate m_{ev}, which may be expressed in the units of $\mathrm{kg\,m^{-3}s^{-1}}$, follows from the interrelation between temperature, moisture content and vapor pressure (i.e., on the sorption isotherms). Values for this combination are not known a priori: they have to be approached during an iterative procedure to establish local equilibrium conditions.

It should be noticed that the mass balance is made for water vapor but not for the total amount of water in the system. Instead, the moisture content u is linked to the mass conservation equation for water vapor by the evaporation rate

$$m_{\mathrm{ev}} = -\rho_{\mathrm{w}}\frac{\mathrm{d}u}{\mathrm{d}t} \tag{5}$$

where ρ_{w} is the density of dry wood.

2.2.3 Constitutive equation for heat transfer

The constitutive equation for conductive heat flux is known as Fourier's first law and can be written as:

$$q = -k_{\mathrm{t}}\nabla T \tag{6}$$

where the conductive heat flux q is the quantity of heat [J] translated through the area of one m^2 during one second. k_{t} denotes the thermal conductivity of the material in the units of $\mathrm{Wm^{-1}K^{-1}}$, considering the porous medium as a homogeneous continuum, and ∇T is the temperature gradient in the flux direction.

2.2.4 Heat conservation equation

Suppose that the four components dry wood, bound water, water vapor, and dry air are named with the subscripts w, b, v and a, respectively. Further, let us introduce the dimensionless mass content $u_i = m_i/m_{\mathrm{w}}$, which gives the local mass ratio of component i to dry wood. Such a denotation, rather than using the density, is convenient to ensure validity of Eq. 7 during compression (and spring-back) of the mat, where the volume of the mat, and consequently the density of each component, changes. It should be noticed that, by definition, the mass content of dry wood, u_{w}, is always 1 and that the mass content of bound water, u_{b}, is the moisture content of wood on a dry weight basis (otherwise symbolized simply as u throughout this paper).

The heat conservation equation for three-dimensional heat flow may be written in a form that follows the formulation of Nasrallah and Perre (1988) for one-dimensional convective drying of porous media:

$$\underset{\text{(conduction)}}{-\nabla q} \underbrace{\underset{\text{(sensible heat)}}{-\nabla\sum_{i=\mathrm{v,a}}(c_i j_i T)} \underset{\text{(phase change)}}{- H_{\mathrm{v}}^{\circ} m_{\mathrm{ev}}}}_{\text{(convection)}} = \underset{\text{(accumulation)}}{\rho_{\mathrm{w}}\frac{\partial}{\partial t}\sum_{i=\mathrm{w,b,v,a}}(c_i u_i T)}\,. \tag{7}$$

The accumulation term on the right hand side describes energy storage, while c_i denotes the specific heat of component i, ρ_{w} the density of dry wood and T the local temperature. The first term on the left hand side describes the conductive heat flow, while the second term expresses the sensible heat transport associated with the mass flow j_i of vapor or air. The third term on the left hand side describes the generation of heat due to phase change, whereby H_{v}° is defined by $H_{\mathrm{v}}^{\circ} = H_{\mathrm{v}} + (c_{\mathrm{b}} - c_{\mathrm{v}})T$. H_{v} denotes the latent heat of sorption from the vapor to the bound water state per unit mass [$\mathrm{Jkg^{-1}}$] and m_{ev} the evaporation rate in the units of $\mathrm{kg\,m^{-3}\ s^{-1}}$; the expression $(c_{\mathrm{b}} - c_{\mathrm{v}})T$ accounts for the difference in specific heat between bound water and water vapor.

A simplified form of Eq. 7 may be derived since the mass of vapor and air within the mat is very small compared to the mass of wood and bound water. Therefore, the transfer of sensible heat associated with the gas flow, as well as heat consumed or liberated when increasing or decreasing the temperature of the gas, may be neglected. The non steady-state heat conservation equation may now be written in the form:

$$\underset{\text{(conduction)}}{-\nabla q} \underset{\text{(phase change)}}{- H_{\mathrm{v}} m_{ev}} = \underset{\text{(accumulation)}}{c_u\rho_u\frac{\partial T}{\partial t}} \tag{8}$$

where c_u and ρ_u, respectively, denote specific heat and density of the wood-furnish material at current moisture content. This heat conservation equation includes conductive heat transfer as well as that share of convective heat transfer that comes from phase change. Convective heat transfer resulting from the transport of sensible heat is neglected. The derivations of Eqs. 4, 7 and 8 are presented in Thömen (2000).

2.2.5 Thermodynamic relationships

The ratio between actual partial pressure of water vapor, p_v, and saturated water vapor pressure, p_{sat}, at a given temperature is described as relative humidity φ. The saturated vapor pressure p_{sat} [Pa] is a function of temperature only and may be calculated according to an empirical equation (Humphrey and Bolton 1989)

$$\log_{10} p_{sat} = 10.745 - \frac{2141.0}{T_{abs}} \tag{9}$$

where T_{abs} is the absolute temperature in K.

As an approximation, the gaseous mixture is assumed to be an ideal mixture of perfect gases. Then, the equation of state of an ideal gas describes the relationships between the thermodynamic properties for each of the gas components i

$$p_i V_{eff} = \frac{m_i}{M_i} R T_{abs}; \quad i = \text{v, a} \tag{10}$$

where v,a = subscripts to denote vapor or air, p_i = partial pressure of component i [Pa], V_{eff} = volume occupied by gas mixture [m^3], m_i = mass of component i [kg], M_i = molecular mass of component i [$kg\,mol^{-1}$], R = gas constant [$J\,mol^{-1}K^{-1}$], T_{abs} = absolute temperature [K].

According to Dalton's law, the total gas pressure, p, of a mixture of ideal gases is equal to the sum of its partial pressures, p_i

$$p = \sum_{i=\text{v,a}} p_i \,. \tag{11}$$

In the present approach vapor (v) and air (a) are assumed to be the only gas components.

Initial and boundary conditions. The wood-furnish mat can consist of one or more discrete layers. Each layer initially has a constant thickness over the x-y plane and a uniform distribution of its conditions and properties.

Three types of spatial boundaries have to be considered: the interface between the composite material and the pressing platen, the interface between composite material and ambient air, and the symmetry planes. The interface between mat and pressing platen is assumed to be impermeable. However, when extending the model to describe a gas injection press, or when considering the mat in front of or behind a continuous press, we have to take into account gas movement through this boundary. The surface temperature of the mat is equal to the platen temperature, which can vary with time according to a specified temperature course. The edges of the mat are open for vapor and air flow. Heat conduction at the edges is unlikely to be of importance and is, therefore, not accounted for.

The mat is always regarded as being symmetrical across its width (y-direction), while symmetries in production (x-direction) and across the thickness (z-direction) are optional. By definition, no heat and mass transfer occurs across symmetry planes.

3 Physical properties

3.1 Material properties

Material property data are specific to the wood-furnish material type. They usually depend greatly on the physical conditions of the material, such as temperature, moisture content and density. Those data used as input data for the simulation program have been determined by two groups working with Humphrey and Fruehwald, respectively, or have been taken from the literature. Only data for MDF fiber material is presented here.

3.1.1 Permeability

Input data for the simulation program consist of two alternative sets of permeability data. Both sets of data give permeability k_p (in m^2) as a function of density ρ (in $kg\,m^{-3}$) and can be expressed by an exponential equation of the form

$$k_p = e^{\frac{1}{a+b\rho+c/\ln\rho}} \,. \tag{12}$$

Coefficients a, b, and c are specified in Table 1.

3.1.2 Obstruction factor for molecular diffusion

The resistance that a porous medium offers to molecular gas diffusion can be expressed by the obstruction factor, k_d. This quantity describes how many times the diffusion resistance of the material exceeds that of an open space devoid of walls. Like k_p, the obstruction factor is a material property that depends upon the pore structure of the medium but is independent of the gas properties.

Table 1 Coefficients for Eq. 12 to determine in-plane and cross-sectional permeability for MDF fiber mats
Tabelle 1 Koeffizienten für Gl. 12 zur Berechnung der horizontalen und vertikalen Permeabilität für MDF-Vliese

	Flow direction	a	b	c
Haselein (1998)	in-plane	−0.006	2.95×10^{-6}	−0.199
	cross-sectional	−0.026	4.98×10^{-6}	−0.074
von Haas et al. (1998)	in-plane	−0.041	9.51×10^{-6}	−0.015
	cross-sectional	−0.037	1.10×10^{-5}	−0.037

Results of steady-state diffusion experiments on MDF samples with homogeneous density profiles have been fitted to an exponential equation to relate the dimensionless obstruction factor in the cross-sectional direction, k_d, to material density ρ in kg m^{-3} (Thömen 2000).

$$k_d = 0.334 e^{5.08\times10^{-3}\rho} . \quad (13)$$

3.1.3 Thermal conductivity

von Haas (1998) described the relation between thermal conductivity perpendicular to the panel plane and density ρ in kg m^{-3} for MDF by

$$k_t^{0.30} = 4.86\times10^{-8}\rho^2 + 4.63\times10^{-5}\rho + 4.38\times10^{-2} \quad (14)$$

where $k_t^{0.30}$ denotes the thermal conductivity in W m^{-1}K^{-1}, measured at 0% moisture content and 30 °C.
Comparison of thermal conductivity versus density curves for different temperatures (von Haas 1998) and moisture contents (Haselein 1998) reveals that the curves follow approximately similar courses that differ by a constant quantity, Δk_t. Therefore, the assumption appears to be justified that, within limits, Δk_t is independent of density and may be added to the values obtained by Eq. 14 to account for moisture and temperature effects. Haselein (1998) evaluated data presented by Shao (1989) and Kühlmann (1962) to derive such a correction term. The expression accounting for moisture u [%] and temperature T [°C] effects may be written as

$$\Delta k_t = 4.9\times10^{-3}u + (1.1\times10^{-4} + 4.3\times10^{-5}u)(T - T_{exp}) \quad (15)$$

with T_{exp} being the average experimental temperature used in the measurements of thermal conductivity (here, 30 °C). Thermal conductivity k_t can then be calculated as a function of density, temperature, and moisture content by combining Eqs. 14 and 15 to yield

$$k_t = k_t^{0.30} + \Delta k_t . \quad (16)$$

Humphrey and Bolton (1989) estimated the effect of heat flux direction relative to the mat's structure on thermal conductivity, based on measurements of Humphrey (1982). They suggested calculating the thermal conductivity parallel to the mat plane, $k_{t,x-y}$, as

$$k_{t,x-y} = 1.5 k_t \quad (17)$$

3.1.4 Specific heat

The specific heat of dry wood, as for many organic materials, appears to increase with increasing temperature. Averaging six equations collected by Skaar (1972) from different authors to account for the temperature effect, and using the method of simple mixtures to account for the moisture content, Haselein (1998) derived the following equation:

$$c = \frac{1131 + 4.19T + 4190u}{1+u} \quad (18)$$

where c = specific heat of wood at current moisture content [J kg^{-1}K^{-1}], T = temperature [°C], u = moisture content, a dimensionless variable

3.1.5 Hygroscopicity

Many researchers have investigated the relationship between equilibrium moisture content (EMC), temperature and relative humidity below 100 °C (e.g. Weichert 1963, Keylwerth 1969), or for elevated temperatures, but vapor pressures below one atmosphere (e.g. Keylwerth 1949, Kollmann and Malmquist 1952). However, only few such data are available for vapor pressures exceeding one atmosphere at elevated temperatures. Apparently, Engelhardt (1979) gave the most comprehensive set of experimental data obtained under such conditions (Fig. 1). The lines of equal relative humidity (sorption isopsychrens) presented by Engelhardt are based on his own measurements in the temperature range between 110 °C and 170 °C, and on measurements reported by Weichert (1963) for temperatures below 100 °C. Both researchers used beech samples for their experiments.

During panel pressing, temperatures in layers of the wood-furnish mat close to the surfaces often exceed 170 °C. Experimental data for such high temperatures are not available, however, so we extrapolated Engelhardt's (1979) curves by fitting a second order polynomial to the measured data and then calculating equilibrium moisture content values for the temperature ranges of 20 to 25 °C and 170 to 220 °C (Fig. 1).

3.1.6 Heat of sorption

The latent heat of sorption[1] is the heat generated per unit mass of water absorbed by wood from the liquid state. Its value is (almost) zero at fiber saturation and increases towards lower moisture contents. If water is absorbed from the gaseous state, the latent heat of evaporation (from the liquid to the gaseous state) has to be added to the latent heat of sorption (from the bound to the liquid state).

The following compound equation presented by Humphrey and Bolton (1989) includes both the latent heat of sorption and the latent heat of evaporation:

$$H = 2.511\times10^6 - 2.48\times10^3 T + 1.172\times10^6 e^{-0.15u} . \quad (19)$$

This expression gives the heat energy required to evaporate a unit of bound water, H in J kg^{-1}, as a function of moisture content u in % and temperature T in °C.

Properties of vapor-air mixtures

Viscosity. For ideal gases, the dynamic viscosity η, hereafter referred to simply as viscosity, is independent of pressure. This

[1] Note: The term 'latent heat of sorption' is used for consistency; it is synonymous with 'differential heat of sorption from the liquid state'.

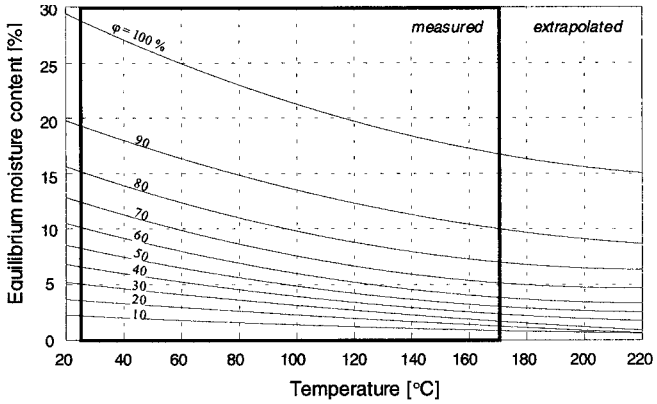

Fig. 1 Measured sorption isopsychrens for beech presented by Engelhardt (1979) and extrapolations
Abb. 1 Gemessene Sorptions-Isopsychren für Buche (nach Engelhardt 1979) und Extrapolation

independence applies to water vapor and air as a good approximation for pressure levels that occur within a wood-furnish mat during pressing. The viscosity of gases rises with increasing temperature as described by the Sutherland equation. From fitting the Sutherland equation to experimental data, Humphrey and Bolton (1989) derived the following expression for the viscosity of water vapor, η_v:

$$\eta_v = \frac{1.12 \times 10^{-5}(T + 273.15)^{1.5}}{T + 3211.0} \tag{20}$$

with η and T in the units of Pa·s and °C, respectively. In the present work the Sutherland equation was fitted to experimental data for air from Munson et al. (1990). The viscosity of air, η_a, is related to temperature by:

$$\eta_a = \frac{1.37 \times 10^{-6}(T + 273.15)^{1.5}}{T + 358.9} \,. \tag{21}$$

In the work presented here, the viscosity of the vapor-air mixture is obtained from a linear combination of the component viscosities weighted by the mole fractions in the mixture. This is only a first order estimate and should be refined in future work to account for the non-linear effect of composition on viscosity.

Molecular diffusion coefficient. The following expression has been derived to relate the binary diffusion coefficient D_{va} of the vapor-air gas pair (in $m^2 s^{-1}$) to the total gas pressure p (in Pa) and absolute temperature T_{abs} (in K):

$$D_{va} = 2.60 \times 10^{-5} \left(\frac{101\,325}{p}\right) \left(\frac{T_{abs}}{298.2}\right)^{1.75} \tag{22}$$

This equation is based on experimental diffusion data presented by Cussler (1984), and on the empirical finding reported by several researchers (Fuller et al. 1966) that the diffusion coefficient is inversely proportional to the total gas pressure and directly proportional to $T^{1.75}$.

4 Numerical procedure

For the numerical solution of the heat and mass transfer model an algebraic approach is employed, in which the set of constitutive flux equations are coupled by local energy and mass balances. Computations for each time step include three distinct consecutive procedures. First, heat and mass fluxes between the mid-points of adjacent control regions are calculated under steady-state conditions to determine the diffusant quantities (e.g., energy) flowing across the interfaces between neighboring regions. Second, knowing gains and losses of the diffusant within each control region, new values for the state variables (e.g., temperature) are calculated. Finally, the state variables are corrected for compression or expansion of the control regions. To improve the efficiency of computations, an adaptive time step scheme in combination with a mechanistic implicit approach for the cross-sectional convective flow calculations was adopted. The differential Eqs. 4,7 and 8 were presented for the sake of completeness, though they are not used here for the numerical solution.

5 Comparison of model predictions with measurements

In order to compare predictions of the simulation model with experimental data, measurements of internal temperature and gas pressure in MDF mats during pressing were made for a large-size (4×8 ft.) laboratory hot press. Furthermore, the specific pressure of the press operated in position control mode was recorded, and density and moisture profile after press opening were determined. Material and methods of these measurements are described in the Appendix. A total of four trials were carried out, with the pressing schedule being the only parameter varied among the four trials. While temperature, gas pressure and moisture content predictions are focused on in the present paper, a comparison of rheological mat behavior and density profile is given in Thömen et al. (2005).

The initial and boundary conditions for the simulations were defined according to the situation in the experiments. A one-layered MDF mat with homogeneous initial mat conditions is

Table 2 Input conditions for simulation
Tabelle 2 Eingabebedingungen für die Simulation

Material:	MDF fiber	Platen temperature:	190 °C
Mat size:	2.30×1.33 m^2	Initial mat temperature:	26 °C
Target thickness:	39 mm	Initial moisture content:	9.9%
Target density[2]:	697 kg/m^3	Density of pre-compressed mat[1]:	92.2 kg/m^3

[1] Density on dry wood basis

considered. The idealized case of first platen-mat contact at $t = 0$ (beginning of the simulation) was assumed for both upper and lower pressing platens. Table 2 and Fig. 2 summarize the main input specifications for trial 1.

Symmetry of the mat in x-, y- and z-direction was assumed, so that computations had to be done for only one eighth of the mat volume. A modeling grid of $6 \times 6 \times 20$ control regions (x, y, z) was used. Test runs showed that a higher resolution in the horizontal plain would not significantly increase the accuracy of the predictions, whereas steep cross-sectional gradients required a high resolution in the z-direction.

5.1 Temperature and gas pressure

In Fig. 3 temperature and gas pressure measured at different spatial positions in the mat are compared with model predictions. A schematic of the mat that shows the positions of the measuring points is displayed in Fig. 6. Bearing in mind the complexity of the problem, the agreement between measurement and prediction can be regarded as good, both qualitatively and quantitatively. All important features of the temperature and gas pressure curves are predicted, including the temperature plateau near 100 °C, the first gas pressure rise during press closure, the final gas pressure increase due to vapor generation, and the gas pressure and temperature drop towards the edges of the mat.

The gas pressure measured at the intermediate position between central plane and surface (P2) is a little higher than that measured at the core (P1). However, for two of the four trials, somewhat lower gas pressures were recorded at P2, compared to P1. Hence, it is reasonable to assume that these differences are artifacts. The gas pressure at P1 and P2 are identical in the simulation, and P2 is therefore not displayed.

The measured gas pressure curves displayed in Fig. 3 are more or less smooth during press closure, while predictions show pronounced peaks that coincide with respective changes of the consolidation rate (see Fig. 2). The explanation for the smooth courses of the measured gas pressures is that the pressing pressure reached its allowed maximum (limited by the press hydraulics) after an elapsed time of between 50 and 100 seconds in trial 1. During this period the pressing pressure dictated the platen position and caused a gliding transition from one to another consolidation rate. In trials 2 and 3 the allowed pressure maximum was not reached; thus the measured gas pressure curves show pronounced peaks, which agree well with those predicted (Fig. 4).

The simulated temperature and gas pressure curves displayed in Fig. 3 somewhat underestimate the measured values. This deviation can be conclusively explained as follows. The actual density profile was more pronounced than the simulated one (see Thömen et al. 2005). As the thermal conductivity is positively re-

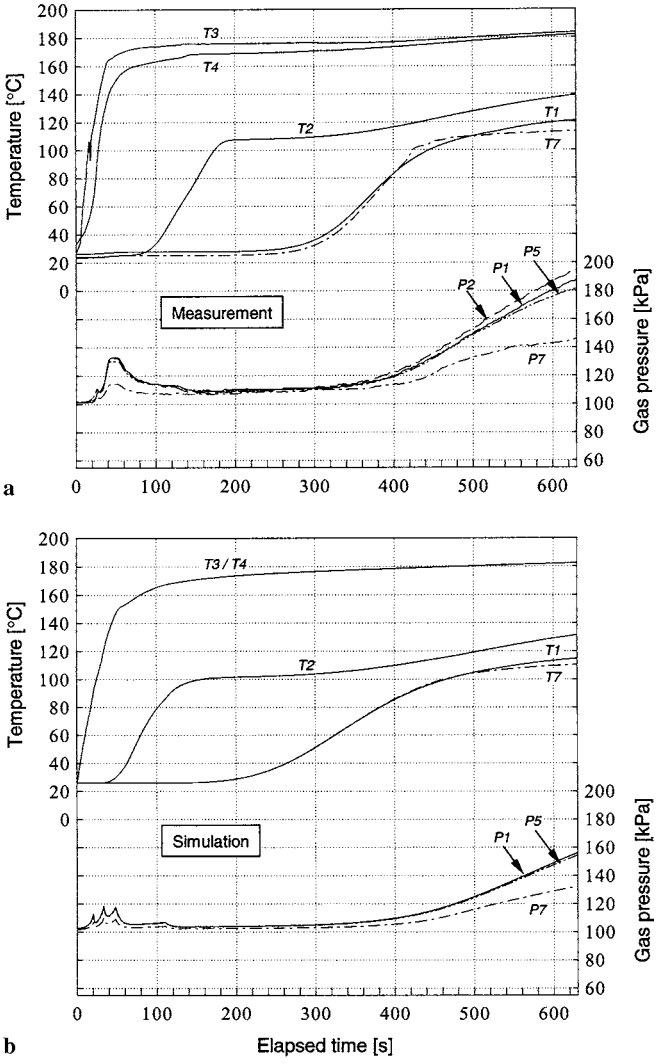

Fig. 3 Comparison of measured (**a**) and predicted (**b**) temperature and total gas pressure development within the mat for trial 1. Positions of sensors are displayed in Fig. 6

Abb. 3 Vergleich der gemessenen (**a**) und vorhergesagten (**b**) Temperatur- und Gasdruckentwicklung innerhalb des Vlieses für Versuch 1. Die Positionen des Sensors sind in Abb. 6 dargestellt

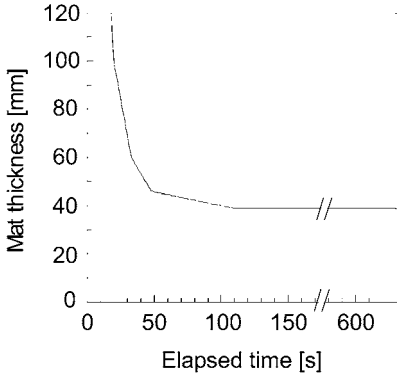

Fig. 2 Specified pressing schedule for trial 1. The initial mat thickness at time $t = 0$ is 295 mm

Abb. 2 Vorgegebenes Pressprogramm für Versuch 1. Die Anfangsdicke der Matte zum Zeitpunkt $t = 0$ beträgt 295 mm

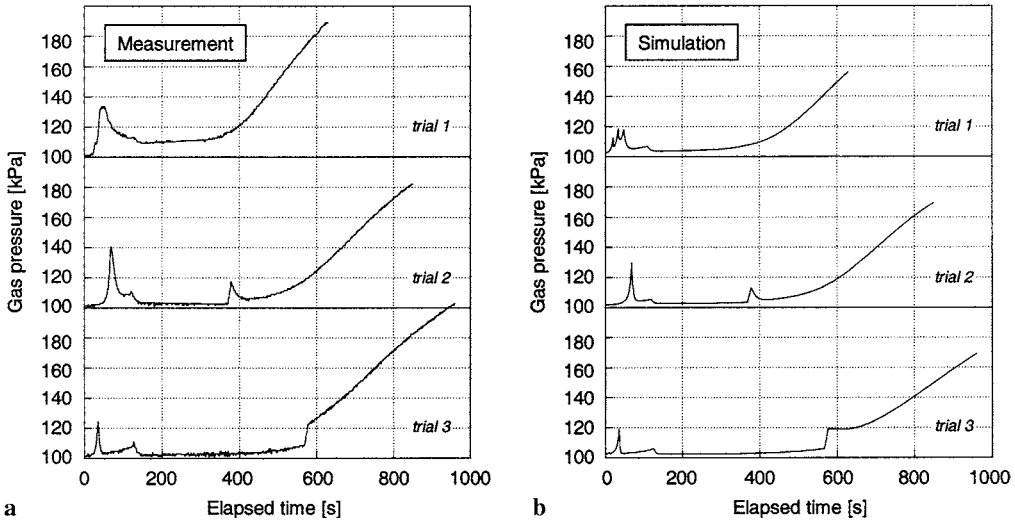

Fig. 4 Comparison of measured (**a**) and predicted (**b**) total gas pressure in the center of the mat (P1 position in Fig. 6). Displayed are curves for trials 1 to 3
Abb. 4 Vergleich des gemessenen (**a**) und vorhergesagten (**b**) Gasdrucks in Vliesmitte (P1-Position in Abb. 6). Dargestellt sind die Kurven für die Versuche 1 bis 3

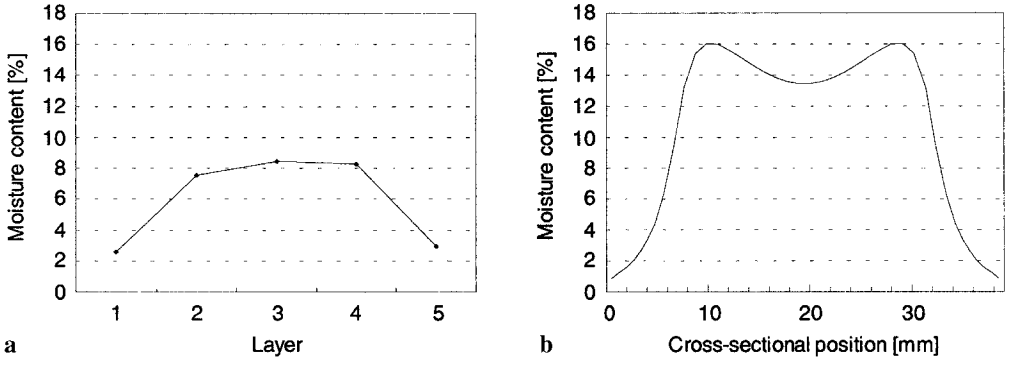

Fig. 5 Comparison of cross-sectional moisture profile in the horizontal center of the panel. (**a**) Measurement for 730 seconds pressing time after press opening. (**b**) Prediction at 630 seconds before press opening (Trial 1)
Abb. 5 Vergleich des Feuchteprofils über den Plattenquerschnitt für die horizontale Plattenmitte. (**a**) Gemessen nach Öffnen der Presse nach 730 Sekunden Presszeit. (**b**) Vorhersage für den Zeitpunkt 630 Sekunden, vor Pressenöffnung. (Versuch 1)

lated to density, higher densities near the surfaces enhance the conductive heat transfer from the pressing platens to the progressing condensation front. To eliminate an error possibly introduced by the density profile prediction, a routine has been implemented within the simulation program that allows model runs with pre-defined density profiles to be executed. An identical simulation of trial 1, but assuming a density profile that reflects the measured one, resulted in significantly higher internal temperatures and gas pressures as those predictions presented in Fig. 3.

5.2 Cross-sectional moisture profile

A pronounced cross-sectional moisture profile develops during the pressing process, with relatively dry surface layers and core moisture contents that, at least temporarily, exceed the initial moisture content. Measured and simulated moisture profiles are presented in Fig. 5. The asymmetry of the curve in Fig. 5a was mainly caused by differences in thickness of the five layers. The displayed moisture profile for the experiment must therefore be regarded only as an approximation of the exact moisture profile.

Measured and predicted cross-sectional moisture profiles show similar trends. Moreover, the M-shape of the predicted profile (Fig. 5b) agrees well with measurements reported by Rackwitz (1954) and Maku et al. (1959). Quantitative accord of the two curves could not be expected for three reasons. First, the simulation was stopped after 630 seconds, while the mat actually stayed in the press for 100 further

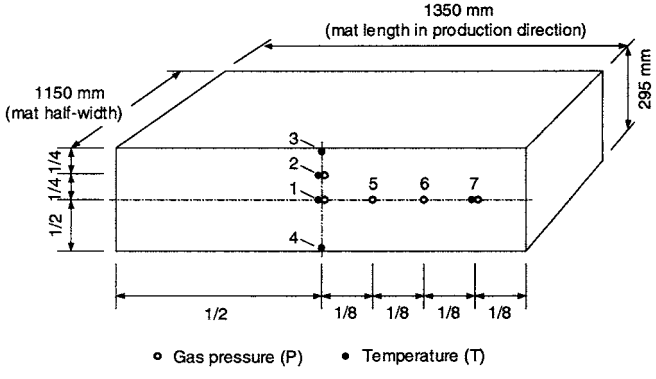

Fig. 6 A vertical cross-section of the mat with positions of temperature and gas pressure probes
Abb. 6 Senkrechter Vliesquerschnitt mit Positionen der Temperatur- und Gasdrucksensoren

seconds of a venting period. Second, vapor escapes from the mat when venting and opening the press, and this leads to a drop in core moisture content. Finally, as mentioned above, the predicted gas pressure lags behind the measured gas pressure. Higher internal gas pressures enhance the vapor escape through the edges, and therefore the overall moisture loss.

6 Conclusions

Measurements in industrial and laboratory pilot trials are usually restricted to only a few positions within the mat. The limited number of measuring points provides information only for specific positions, while a coherent picture of the physical conditions inside the mat may be difficult to derive from the discrete data. Furthermore, some variables, such as moisture content or material properties, are difficult or impossible, so far, to measure during the process. These limitations do not hold for theoretical simulation models. In principle, all variables included in the model may be output and displayed for any location and for the entire time period that is simulated. This is one of the reasons why simulation models are so widespread in most engineering fields, and almost certainly will continue to gain importance in the future.

While only a relatively short demonstration of predictions generated with the simulation model, and of comparisons with experimental data, could be delivered in this paper, a much wider range of events in the pressing process may be illuminated by simulation. Of particular interest are those questions that have been difficult in the past to address solely by experiment. In this respect, the simulation model presented here is an important tool not only for the short range optimization of the industrial process, but also to improve our understanding of the complex interactions during hot pressing in the long term.

Critical for the use of hot-pressing models are, among others, the availability of appropriate material property input data. A list of such data has been included in this paper. However, for the future it is not enough to characterize only a few material types. The material properties of the wood-furnish material strongly depend on the wood species mix, as well as on the size distribution and shape of the wood particles. Both the species mix and the geometry of the particles vary considerably between materials from different manufacturers, and new material types will be added in the future. Consequently, the development of methods to easily determine the characteristics of any new material must be an ongoing objective.

Acknowledgement The authors are grateful to G. Siempelkamp GmbH & Co. for facilitating our access to their laboratory for hot pressing experiments. This work was supported by USDA funds through the Center for Wood Utilization at Oregon State University and by the Federal Ministry of Economics and Technology (Germany) through the German Wood Research Foundation (DGfH). The authors also acknowledge the encouragement of Drs. A. Fruehwald and A. Steffen.

References

Bolton AJ, Humphrey PE (1994) The permeability of wood-based composite materials. Part I. A review of the literature and some unpublished work. Holzforschung 48(Suppl.):95–100

Carvalho LMH, Costa CAV (1998) Modeling and simulation of the hot-pressing process in the production of medium density fiberboard (MDF). Chemical Engineering Communications, Gordon & Breach Science Publ Inc., 170:1–21

Carvalho LMH, Costa MRN, Costa CAV (2003) A global model for the hot-pressing of MDF. Wood Sci Technol 37:241–258

Cussler EL (1984) Diffusion. Mass transfer in fluid systems. Cambridge Univ. Press., pp 525

Dai C, Yu C (2004) Heat and mass transfer in wood composite panels during hot-pressing: Part I. A physical-mathematical model. Wood Fiber Sci 36(34):585–597

Denisov OB, Anisov PP, Zuban PE (1975) Untersuchung der Permeabilität von Spanvliesen. Holztechnologie 16(1):10–14

Engelhardt F (1979) Untersuchungen über die Wasserdampfsorption durch Buchenholz im Temperaturbereich von 110 °C bis 170 °C. Holz Roh-Werkst 37:99–112

Fuller EN, Giddings JC, Schettler PD (1966) A new method for prediction of binary gas-phase diffusion coefficient. J Int Eng Chem 58(1):19–27

Garcia PJ (2002) Three-dimensional heat and mass transfer oriented strandboard hot-pressing. Ph.D. Thesis, Univ. of British Columbia, Canada, pp 254

Gefahrt J (1977) Zur Spänevorwärmung mit Hochfrequenzenergie – Modell zur Berechnung des Temperaturverlaufes in Vliesmitte bei der Heißpressung. Holz Roh- Werkst 35:183–188

von Haas G (1998) Untersuchungen zur Heißpressung von Holzwerkstoffmatten unter besonderer Berücksichtigung des Verdichtungsverhaltens, der Permeabilität, der Temperaturleitfähigkeit und der Sorptionsgeschwindigkeit. Dissertation, Univ. Hamburg, Germany, pp 264

von Haas G, Steffen A, Frühwald A (1998) Untersuchungen zur Permeabilität von Faser-, Span- und OSB-Matten für Gase. Holz Roh- Werkst 56(2):386–392

Haselein CR (1998) Numerical simulation of pressing wood-fiber composites. Ph.D. Thesis, Oregon State Univ., U.S.A., pp 244

Heinemann C (2004) Charakterisierung der Aushärtung von Aminoharzen in einer Holzpartikelmatrix durch Evaluierung von Festigkeiten und Reaktionskinetik. Ph.D. Thesis, Univ. of Hamburg, pp 236

Hubert P, Dai C (1998) An object-oriented finite element processing model for oriented strand board wood composites. Proc. of the 13th Int. Conf. on Composite Materials, Paris, France

Humphrey PE (1982) Physical aspects of wood particleboard manufacture. Ph.D. Thesis, Univ. of Wales, UK

Humphrey PE (1999) Bonding speed of adhesives: an automated evaluation system. Pullman WA, Wolcott M (eds) In: Proc. 33rd. International Particleboard and Composite Materials Symp., Pub. Washington State Univ., pp 139–146

Humphrey PE, Bolton AJ (1989) The hot pressing of dry-formed wood-based composites. Part II. A simulation model for heat and moisture transfer. Holzforschung 43(3):199–206

Keylwerth R (1949) Grundlagen der Hochtemperaturtrocknung des Holzes. Holzzentralblatt 75:953–954

Keylwerth R (1969) Praktische Untersuchungen zum Holzfeuchtigkeits-Gleichgewicht. Holz Roh- Werkst 27(4):285–290

Kollmann F, Malmquist L (1952) Untersuchungen über die Trocknung von Kiefernholz mit erhöhten Temperaturen. Svenska Traforsk, Tratekn Avd 23

Krischer O (1963) Die wissenschaftlichen Grundlagen der Trocknungstechnik. 2nd edn. Springer-Verlag, Berlin, pp 491

Kühlmann G (1962) Untersuchungen der thermischen Eigenschaften von Holz und Spanplatten in Abhängigkeit von Feuchtigkeit und Temperatur im hygroskopischen Bereich. Holz Roh- Werkst 20:259–270

Maku T, Sasaki R, Hamada H (1959) Studies on the particle board. Report IV. Temperature and moisture distribution in particle board during hot-pressing. Wood Res 21:34–46

Munson BR, Young DF, Okiishi TH (1990) Fundamentals of fluid mechanics. Wiley, New York, p 843

Nasrallah SB, Perre P (1988) Detailed study of a model of heat and mass transfer during convective drying of porous media. Int J Heat Mass Transfer 31(1):957–967
Nigro N, Storti M (2001) Hot-pressing process modeling for medium density fiberboard (MDF). Int J Math Math Sci 26(6):713–730
Rackwitz G (1954) Ein Beitrag zur Kenntnis der Vorgänge bei der Verleimung von Holzspänen zu Holzspanplatten in beheizten hydraulischen Pressen. Dissertation, Technische Hochschule Braunschweig, Germany
Shao M (1989) Thermal properties of wood fiber networks. MS Thesis, Oregon State Univ., USA, pp 95
Skaar C (1972) Water in wood. Syracuse University Press, New York, p 218
Steffen A (1996) Entwicklung und Stand der Optimierung und Modellierung der Heißpressung von Holzwerkstoffmatten. Holz Roh- Werkst 54:321–332
Thoemen H (2000) Modeling the Physical Processes in Natural Fiber Composites During Batch and Continuous Pressing. Ph.D. Thesis, Oregon State Univ., USA, pp 187
Thoemen H, Humphrey PE (2003) Modeling the continuous pressing process for wood-based composites. Wood Fiber Sci 35(3):456–468
Thoemen H, Haselein CR, Humphrey PE (2005) Modeling the physical processes relevant during hot pressing of wood-based composites. Part II. Rheology (Submitted to Holz Roh- Werkst)
Weichert L (1963) Untersuchungen über das Sorptions- und Quellungsverhalten von Fichte, Buche und Buchen-Preßvollholz bei Temperaturen zwischen 20 °C und 100 °C. Holz Roh- Werkst 21:290–300
Zombori BG (2001) Modeling the transient effects during the hot-compression of wood-based composites. PhD Thesis. Virginia State Univ., USA, pp 212

Appendix: Measurements in a large-size laboratory press

A Material and methods

Measurements of internal temperature and gas pressure during pressing of MDF in a 4×8 ft. laboratory press were carried out to provide experimental data that can be used to validate the simulation model. The resinated fiber mats used for the experiments were produced in an industrial MDF plant from pine chips (8.2 bar digester pressure). A melamine-supplemented urea-formaldehyde resin (UFm) was used as the adhesive. Four fiber mats were taken from the conveyer belt between pre-press and hot press and then transported within 4 hours to the laboratory to be pressed. Mat 1 was consolidated about eight hours and mats 2, 3 and 4 twenty-six to thirty hours after mat forming.

The mat's dimensions were about $1350 \times 2300 \times 295\ mm^3$, and moisture contents prior to pressing were measured as 9.4% to 11.1% (9.9% for mat 1). Five thermocouples and five thin stainless steel tubes (inside diameter 0.5 mm, outside diameter 1.0 mm) were inserted from the right side into the loose mat, following the scheme shown in Fig. 6. The tubes were connected to small pressure transducers. About 5 minutes after press opening, $50 \times 50\ mm^2$ samples were cut from the center and the edge of each panel to determine cross-sectional density and moisture profiles. A commercial X-ray densitometer was used for the density profile measurements. The samples for the moisture content measurements were immediately sub-divided into five or six slices parallel to the panel surface and put into plastic bags to avoid further moisture changes.

The laboratory batch press was operated in position control mode. The pressing cycle was the only parameter that was specifically varied between the four trial measurements. All panels were pressed to a target thickness and density of 39 mm and $700\ kg/m^3$, respectively. While the press was closed to its final position early in trial 1, the other mats reached its final thickness only in a second densification step after 370 s (trial 2) or 570 s (trial 3 and 4), respectively. Trials 3 and 4 were almost identical; they only differed in the pressing time. The target platen temperature was 190 °C; actual temperatures varied between 186 °C and 192 °C.

B Results

Temperature and gas pressure readings for trial 1 are displayed in Fig. 3a, while Fig. 5a shows the final cross-sectional moisture distribution for this trail. The measured total gas pressure in the center of the mat has been summarized for trials 1 to 3 in Fig. 4a. The interested reader is referred to Thömen (2000) for a comprehensive set of experimental data for trials 1 to 4.